JACS
JOURNAL OF THE AMERICAN CHEMICAL SOCIETY
Article
Cite This: J. Am. Chem. Soc. 2019, 141, 3470−3479
pubs.acs.org/JACS

Atomic Scale Evidence of the Switching Mechanism in a Photomagnetic CoFe Dinuclear Prussian Blue Analogue

Sadaf Fatima Jafri,[†] Evangelia S. Koumousi,[‡,§,∥,⊥] Marie-Anne Arrio,[*,†] Amélie Juhin,[†] Dmitri Mitcov,[∥,⊥] Mathieu Rouzières,[∥,⊥] Pierre Dechambenoit,[∥,⊥] Dongfeng Li,[#] Edwige Otero,[▽] Fabrice Wilhelm,[○] Andrei Rogalev,[○] Loïc Joly,[▽,◆] Jean-Paul Kappler,[▽,◆] Christophe Cartier dit Moulin,[¶] Corine Mathonière,[*,‡,§] Rodolphe Clérac,[∥,⊥] and Philippe Sainctavit[*,†,▽]

[†]IMPMC, CNRS, Sorbonne Université, IRD, MNHN, UMR7590, F-75005 Paris, France
[‡]CNRS, ICMCB, UMR5026, F-33600 Pessac, France
[§]Univ. Bordeaux, ICMCB, UMR5026, F-33600 Pessac, France
[∥]CNRS, CRPP, UMR5031, F-33600 Pessac, France
[⊥]Univ. Bordeaux, CRPP, UMR5031, F-33600 Pessac, France
[#]College of Chemistry, Central China Normal University, 430079 Wuhan, P. R. China
[▽]Synchrotron SOLEIL, L'Orme des Merisiers, F-91192 Saint-Aubin, France
[○]European Synchrotron Radiation Facility, BP 220, F-38043 Grenoble, France
[◆]Université de Strasbourg, CNRS, IPCMS, UMR7504, F-67000 Strasbourg, France
[¶]Sorbonne Université, CNRS, UMR8232, IPCM, F-75005 Paris, France

Supporting Information

ABSTRACT: Molecular complexes based on Prussian Blue analogues have recently attracted considerable interest for their unique bistable properties combined to ultimately reduced dimensions. Here, we investigate the first dinuclear FeCo complex exhibiting both thermal and photomagnetic bistability in the solid state. Through an experimental and theoretical approach combining local techniques—X-ray absorption spectroscopy (XAS), X-ray magnetic circular dichroism (XMCD), and ligand field multiplet calculations—we were able to evidence the changes occurring at the atomic scale in the electronic and magnetic properties. The spectroscopic studies were able to fully support at the atomic level the following conclusions: (i) the 300 K phase and the light-induced excited state at 4 K are both built from $Fe^{III}_{LS}-Co^{II}_{HS}$ paramagnetic pairs with no apparent reorganization of the local structure, (ii) the 100 K phase is composed of $Fe^{II}_{LS}-Co^{III}_{LS}$ diamagnetic pairs, and (iii) the light-induced excited state is fully relaxed at an average temperature of ≈50 K. In the paramagnetic phase at 2 K, XAS and XMCD reveal that both Fe and Co ions exhibit a rather large orbital magnetic moment (0.65 μ_B and 0.46 μ_B, respectively, under an external magnetic induction of 6.5 T), but it was not possible to detect a magnetic interaction between spin centers above 2 K.

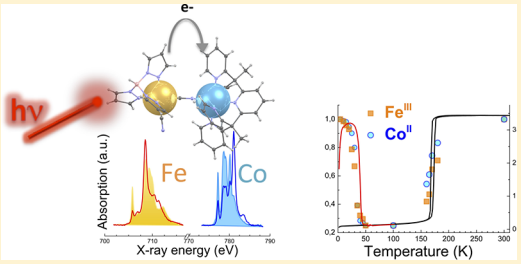

INTRODUCTION

With growing technological interests, smart molecular materials with reduced dimensions[1−4] are being designed, synthesized, and investigated for computing applications,[5] which include, for instance, switching devices,[6] data storage and processing,[7] and logic gates.[8] In these applications, a single molecule is employed to perform numerous binary operations based on logic. Molecular complexes exhibiting externally controlled properties are well-suited for these applications because of their flexible and versatile chemistry. The on−off switching capability between two molecular states, for example, magnetic (on or 1) and diamagnetic (off or 0) states is termed as bistability. This switching phenomenon can be used to store data as binary units "0" and "1" if the molecules possess a memory effect under external stimuli (light, temperature, magnetic field, pressure, etc.). To develop such switchable molecules using state-of-the-art chemistry, careful manipulation and tailoring of the molecular properties, with control down to a single spin carrier, is a current challenge.[4,9−11] In this regard, the versatile molecular chemistry of mixed valence cyanido-bridged Prussian Blue ($Fe^{II}-CN-Fe^{III}$) and its derivatives ($A^{II/III}-CN-B^{III/II}$, where A and B are 3d transition-metal ions, noted as AB in the following), referred

Received: September 28, 2018
Published: December 2, 2018

DOI: 10.1021/jacs.8b10484
J. Am. Chem. Soc. 2019, 141, 3470−3479

to as Prussian Blue analogues (PBA), has been exploited to engineer bistable systems.[12] The first evidence of light-induced magnetism in a three-dimensional (3-D) network of FeCo PBA by Hashimoto and co-workers[13] fuelled the quest for designing photoswitchable molecule-based magnets with novel functionalities in this family. FeCo PBA magnets are unique systems exhibiting bistability due to an electron transfer that transforms Fe^{II}_{LS} (S = 0)−CN−Co^{III}_{LS} (S = 0) diamagnetic entities into Fe^{III}_{LS} (S = $^1/_2$)−CN−Co^{II}_{HS} (S = $^3/_2$) paramagnetic ones (LS = low spin, HS = high spin). This metal-to-metal electron transfer via the cyanido bridge can be tuned by external parameters like light, temperature, and pressure.[11,13−18] Reducing the dimensionality of the material allows the device miniaturization, which is the ultimate goal. The first step was to develop molecular complexes of PBA with the desired thermal and photoinduced electron transfer properties. Some attempts have been made to synthesize cyanide FeCo complexes, but thermal- and/or photoinduced electron transfer properties could not be observed.[19−21] The first evidence of thermally induced metal-to-metal electron transfer was reported in a pentanuclear cyanido-bridged [Fe_2Co_3] molecule by Dunbar and co-workers in 2004.[22,23] More recently, PBA-based [Fe_nCo_n] nanostructures, such as one-dimensional (1-D) networks[24−28] and molecular cubes,[29] squares,[30−35] and dinuclear pairs,[36,37] have also been synthesized. However, only a few systems have been fully characterized by structural methods in their light-induced metastable state.[33,38−40] Furthermore, there are not many examples where the light-induced electron transfer is observed at the atomic scale using XAS/XMCD techniques.[41−45]

Recently, Koumousi et al. succeeded in synthesizing the first dinuclear complex that exhibits both thermo- and photomagnetic bistabilities in the solid state.[37] This dinuclear complex is assembled from $[TpFe(CN)_3]^-$ and $[Co(PY5Me_2)]^{2+}$ building blocks [Tp = hydridotris(pyrazol-1-yl)borate, $PY5Me_2$ = 2,6-bis(1,1-bis(2-pyridyl)ethyl)pyridine] and it can be seen as the elementary motif of the FeCo PBA (see Figure 1). At room temperature, the FeCo dinuclear complex in its desolvated form is in its Fe^{III}_{LS} (S = $^1/_2$)−CN−Co^{II}_{HS} (S = $^3/_2$) paramagnetic state and it undergoes a transition around 167 K toward the Fe^{II}_{LS} (S = 0)−CN−Co^{III}_{LS} (S = 0) diamagnetic state. At low temperature (below 10 K) and under white light irradiation, the diamagnetic pairs undergo a light-induced conversion toward the Fe^{III}_{LS} (S = $^1/_2$)−CN−Co^{II}_{HS} (S = $^3/_2$) paramagnetic state. A characteristic increase of χT product (χ being the magnetic susceptibility) under light irradiation is observed, and within 4 h of irradiation a maximum value of 2.8 cm^3 K mol^{-1} is reached as expected for the paramagnetic FeCo pair. The electron transfer process is complete and reversible, and for the first time this was observed in a dinuclear system.[12,37] All of the above-mentioned changes of the electronic configurations driven by electron transfer have been proposed to explain the variation of the magnetic susceptibility measured by conventional magnetometry.[37] However, there has been so far no direct confirmation at the atomic level that such an electron transfer between Co and Fe sites does indeed take place. Therefore, we have investigated the modifications of the electronic and magnetic structures in temperature and under light irradiation using X-ray absorption spectroscopy (XAS) and X-ray magnetic circular dichroism (XMCD), which are element-specific, synchrotron-based techniques. The goal of this spectroscopic study is to determine the properties of the Fe and Co ions in the three phases involved in the photomagnetic mechanism: the 300 K paramagnetic phase, the 100 K diamagnetic phase, and the 4 K photoinduced paramagnetic phase. The analysis of the XAS and XMCD experimental data is supported by ligand field multiplet (LFM) calculations[46] developed by Thole and magneto-optical sum rules[47,48] in order to determine the orbit and spin magnetic moments of Fe and Co in the 4 K photoinduced paramagnetic phase. The nature of the magnetic coupling between Fe and Co ions in the dinuclear complex was also investigated using element-specific magnetization curves measured by XMCD.

Previously, element-specific and surface-sensitive XAS has been successfully employed to understand the bistability in other molecular systems, such as spin crossover (SCO) systems,[49−51] or cobalt−dioxolene valence tautomers.[41,42,52,53] In SCO compounds, one follows a high spin (HS) to low spin (LS) conversion centered on the same metallic ion, while in cobalt−dioxolene valence tautomers, an electron transfer takes place between a cobalt ion and the dioxolene ligand accompanied by a high spin to low spin conversion of the Co center. In PBAs and molecular analogues, a metal-to-metal electron transfer via cyanido ligands is accompanied also by a high spin to low spin conversion of the Co ions.[12,43,54−59] Investigation of thermo- and photoinduced electron transfer by XAS has been reported by Sekine et al. on discrete systems of FeCo PBA.[43,59] The originality of the present results stems from the recording of XAS and XMCD spectra for both metallic ions involved in the electron transfer on the same sample, thus providing a direct, atomic-scale picture of the switching mechanism and possible information on the nature of the magnetic coupling between metal centers in the light-induced metastable phase.

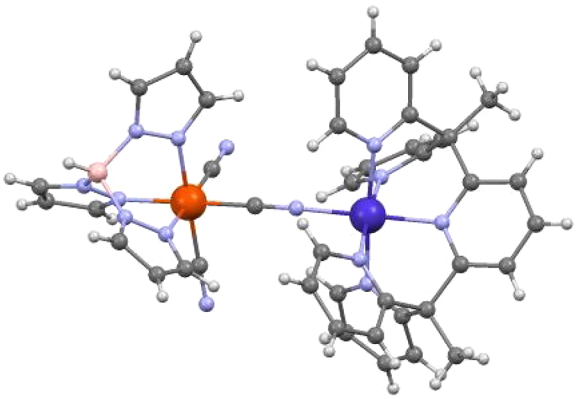

Figure 1. Molecular structure of the cationic complex of the dinuclear FeCo PBA $[(Tp)Fe(CN)_3Co(PY5Me_2)]^+$, where Tp = hydridotris(pyrazol-1-yl)borate and $PY5Me_2$ = 2,6-bis(1,1-bis(2-pyridyl)ethyl)pyridine. All anions, lattice solvents, and hydrogen atoms are omitted for clarity. Fe, Co, N, C, B, and H atoms are indicated in orange, dark blue, light blue, gray, pink, and white, respectively.

EXPERIMENTAL SECTION

Sample Preparation. The desolvated FeCo dinuclear complex with formula $[(Tp)Fe^{III}(CN)_3Co^{II}(PY5Me_2)](OTf)$ [referred to as compound **1**, (OTf = CF_3SO_3, trifluoromethanesulfonate)] and the corresponding Fe and Co precursors were synthesized following the procedure reported by Koumousi et al.[37] The chemical formulas for Fe and Co precursors are $(NBu_4)[(Tp)Fe^{III}(CN)_3]$, labeled compound **2**, and $[Co^{II}(PY5Me_2)H_2O](BF_4)_2$, labeled compound **3**,

DOI: 10.1021/jacs.8b10484
J. Am. Chem. Soc. 2019, 141, 3470−3479

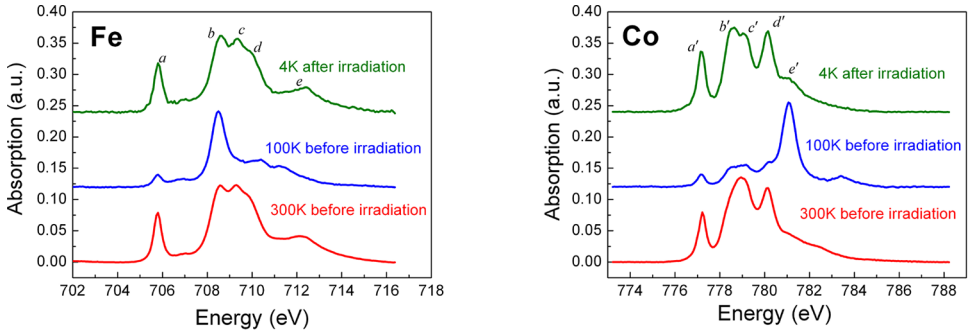

Figure 2. Experimental XAS spectra at the Fe (left) and Co (right) L_3 edge before LED irradiation at 300 K (red line), 100 K (blue line), and 4 K after irradiation (green line) (λ = 660 nm, P = 19 mW/cm^2, 2 h) at **B** = 2 T.

respectively. For **1**, the metal-to-metal electron transfer in the solid state was previously studied using standard magnetometric techniques, single crystal diffraction, and optical reflectivity methods [see the work by Koumousi et al.[37] and the Supporting Information (SI)].

XAS and XMCD Measurements. A powder sample of **1** was deposited on a double-sided conductive carbon tape suitable for cryogenic temperatures and mounted on a copper sample holder. XAS and XMCD measurements were performed at both $L_{2,3}$ and K edges of Fe and Co ions. Spectra at the $L_{2,3}$ edges were recorded on two soft X-ray beamlines, the DEIMOS (SOLEIL synchrotron, France)[60] and the SIM (SLS synchrotron in Switzerland) beamlines.[61,62] All spectra at $L_{2,3}$ edges were measured by recording the total electron yield (TEY) under ultrahigh vacuum conditions. K edge XAS spectra were recorded at the ID12 beamline[63,64] (ESRF synchrotron, France) by measuring the total fluorescence yield.

The DEIMOS beamline is equipped with a 7 T cryomagnet that has a variable-temperature insert. To avoid any spurious signals, the XMCD signal was measured by taking the difference of two XAS spectra recorded for left- and right-polarized X-rays with the propagation vector parallel or antiparallel to the direction of external magnetic induction **B**. By definition, the XMCD signal is obtained by $\sigma_{XMCD} = \sigma^- - \sigma^+$ where $\sigma^- = [\sigma_L(B^-) + \sigma_R(B^+)]/2$ and $\sigma^+ = [\sigma_L(B^+) + \sigma_R(B^-)]/2$.[65] XAS and XMCD spectra for **1** were first recorded at 300, 100, and 4 K to check for thermal-induced conversion. At 4 K, the sample was irradiated with a LED (λ = 660 nm and P = 19 mW/cm^2) for 2 h and the photoconverted state was recorded. We also followed the relaxation of the light-induced excited state when the temperature was raised up to 50 K. The reversibility of the thermo- and photoinduced conversion has been carefully checked by recording XAS spectra for temperatures between 100 and 300 K.

To check for the nature of the magnetic coupling between the Fe and Co ions in the photoinduced state, XMCD signals should be measured in subkelvin temperature because the Fe−Co exchange coupling is expected to be small. On the SIM beamline, the French TBT-mK cryomagnet is a unique tool to perform XMCD measurements in the subkelvin range down to 300 mK.[61] However, due to technical issues, the measurements could only be performed at 2 K. At 2 K, the sample was irradiated using a 660 nm LED (P = 19 mW/cm^2) and the XMCD signal of the photoexcited paramagnetic state was measured. Thanks to XMCD, it is possible to record magnetization curves that are specific to the absorbing ion by setting the energy of the monochromator at the maximum (in absolute value) of the XMCD signal and then sweeping the intensity of the magnetic induction. As can be deduced from the magneto-optical sum rules, the variation of the XMCD intensity at the $L_{2,3}$ edges is a measure of the magnetization of the absorbing atom.

At the ID12 beamline, Fe and Co K edge XAS spectra were measured at 300 and 2 K. At 2 K, compound **1** was irradiated for 3 h by the white light delivered by a tungsten halogen lamp (P = 0.5 mW/cm^2) and then Fe and Co K edge spectra were measured in the photoexcited state.

Ligand Field Multiplet Calculations. Quantitative information from the XAS and XMCD spectra can be extracted by using ligand field multiplet (LFM) calculations.[46,66,67] These calculations are performed by employing the theory which has been developed by Thole,[46] based on an atomic theory by Cowan[68] and for which the crystal-field interactions (i.e., symmetry) are described following Butler's work.[69] We have performed LFM calculations to simulate the Co and Fe $L_{2,3}$ edges spectra in octahedral or distorted environments. The parameters of the calculations are reported in Table S1 (SI). The core-hole lifetime is mimicked by a Lorentzian broadening for which the half-width at half maximum is 0.25 eV at the L_3 edge and 0.50 eV at the L_2 edge. The instrumental Gaussian broadening is σ = 0.1 eV. The definitions of Dq, Dσ, and Dτ parameters can be found in the paper by Juhin et al.[70] Configuration interaction has been used for the calculation of the Fe and Co $L_{2,3}$ edges. The definitions for the associated parameters are best found in de Groot and Kotani's book with precisions on the phase convention for V_{eg} and V_{t2g}.[67] For the calculations, the magnetic field is applied along the direction of the photon **k** vector. The XAS and XMCD signals for powders are obtained by averaging the direction of the **k** vector over the unit sphere with respect to the crystal field axes.

The analysis of the LFM calculations yields the spin and orbital magnetic moments for both Co and Fe ions.

RESULTS

Thermally Induced and Light-Induced Metal-to-Metal Electron Transfer. Figure 2 shows the XAS experimental spectra at the Fe and Co L_3 edges for **1** at 300 and 100 K before LED irradiation and at 4 K after LED irradiation (λ = 660 nm). At 300 K, the spectral shape is characteristic of Fe^{III}_{LS} and Co^{II}_{HS} metal ions.[71−73] Peak *a* on the Fe L_3 XAS spectrum is the electronic signature of Fe^{III}_{LS} ions surrounded by cyanido ligands, and peaks *a*′ to *d*′ on the Co L_3 XAS spectrum are mainly the contribution from Co^{II}_{HS}.[71] When **1** is cooled down to 100 K, peak *b* at the Fe L_3 edge and peak *e*′ at the Co L_3 edge become the main features. Both *b* and *e*′ peaks can be respectively associated with Fe^{II}_{LS} and Co^{III}_{LS} metal ions, thus confirming the temperature-induced switching mechanism proposed from conventional magnetic susceptibility measurements.[37] Nevertheless at 100 K, *a*, *a*′, *b*′, and *c*′ peaks have not completely disappeared, which implies that the electronic conversion is not complete for both Fe and Co ions. One can estimate that around 25% of the high-temperature phase is still present at 100 K. This percentage is determined by linear combinations of LFM reference spectra calculated for Co^{II}_{HS}, Co^{III}_{LS}, Fe^{II}_{LS}, and Fe^{III}_{LS} metal ions.[55] Then, **1** is further cooled down to 4 K and irradiated at 660 nm. From a straightforward comparison with the XAS signature at 300 K and with experimental and theoretical results from the literature,[44,55,57,71,72,74] it is clear that the light-induced state

DOI: 10.1021/jacs.8b10484
J. Am. Chem. Soc. 2019, 141, 3470−3479

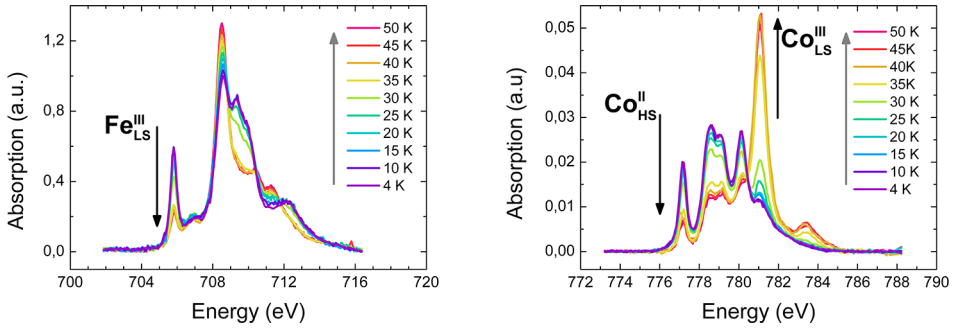

Figure 3. L_3 edge XAS spectra measured in compound **1** for Fe (left) and Co (right), following the relaxation of the light-induced Fe^{III}_{LS}–Co^{II}_{HS} excited state as a function of temperature at ca. 0.1 K/mn, under **B** = 2 T.

is built from paramagnetic Fe^{III}_{LS} and Co^{II}_{HS} species. The respective contributions of low spin and high spin characteristic features in the Fe and Co L_3 XAS spectra therefore clearly confirm the existence of thermo- and photoinduced electron transfers.

Thermal Relaxation of the Photoinduced Excited State. We have recorded the relaxation of the photoexcited state toward the thermodynamically stable diamagnetic state when the temperature is increased. Compound **1** was first cooled down to 4 K and irradiated at 660 nm (P = 19 mW/cm^2). Then the temperature was raised from 4 to 10 K and then from 10 to 50 K in steps of 5 K (the temperature rate is less than 0.1 K/mn), and at each temperature point, Fe and Co L_3 edges spectra have been recorded (Figure 3). When the temperature increases, one observes a gradual decrease of the main signature of Fe^{III}_{LS} (peak a) and Co^{II}_{HS} (peak a') metal ions. As mentioned before, at 100 K the signals for Fe and Co before and after irradiation/thermal relaxation are composed of ≈75% of Fe^{II}_{LS}–Co^{III}_{LS} diamagnetic pairs and 25% of residual Fe^{III}_{LS}–Co^{II}_{HS} paramagnetic pairs. At a given temperature, each spectrum is analyzed as a linear combination of the spectra measured at T = 4 and 100 K (Figure S1 (SI) reports in more detail the fitting procedure), and this method allows the determination of the fraction of each metal ion as a function of temperature (Figure 4). One can observe that the relaxation curves for Fe and Co are almost identical, indicating that the reduction of Fe ions is accompanied by the oxidation of Co ions, as expected for the electron transfer mechanism. The relaxation is almost complete at 50 K. In Figure 4, the size of the symbols is a rough estimate of the errors on the x-axis (≤5 K) and on the y-axis (≈ 5%) that arise respectively from the temperature stabilization of the coldfinger and from the dynamic relaxation during the recording process.

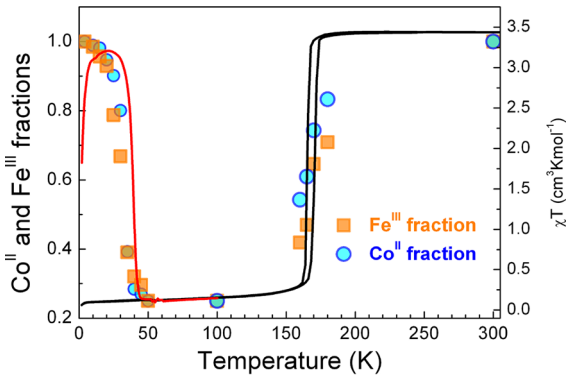

Figure 4. Fraction of the paramagnetic Co(II) and Fe(III) metal ions as a function of temperature, extracted from the quantitative analysis of XAS spectra measured at the Fe and Co L_3 edge (0.1 K/min). The size of the symbols accounts for the error bars on the x- and y-axes. For comparison, the χT product vs T is plotted. χT is obtained from conventional magnetization measurements (0.4 K/min), in the dark (black solid line) and in the dark after white light excitation (P = 3 mW/cm^2) at 10 K (red solid line).

A similar series of measurements were performed between 100 and 300 K for intermediate temperatures equal to 160, 165, 170, and 180 K. The percentage of each species was determined from the linear combination of the reference spectra measured at 100 and 300 K (Figure 4).

For comparison, the experimental variation of the magnetic susceptibility (shown as χT) measured by conventional magnetometry is shown in Figure 4. The χT product for a paramagnetic species is independent of temperature in the case of a Curie behavior: it is zero for a diamagnetic pair and equals ca. 3 cm^3 K mol^{-1} for the Fe^{III}_{LS}–Co^{II}_{HS} paramagnetic pair. The agreement between XAS and magnetic measurements is quite good, and both techniques observe the complete relaxation of the photoinduced state around 48 K and the thermally induced conversion around 165 K (see Figure S2 of the SI for complementary information).

Reversibility of the Electron Transfer Process. One major point was to check whether the spectral modifications observed with temperature and light irradiation were fully reversible, in order to discard any degradation of the sample that could explain these changes. Starting from the light-induced state at 4 K, we have warmed up **1** and recorded XAS spectra at 100 and 300 K. By doing so, **1** has followed a complete temperature cycle: 300, 100, 4 K and irradiation at 660 nm, 100 K, and eventually 300 K. Spectra recorded at 100 K before and after the 10 K photomagnetic conversion/thermal relaxation are almost identical at both the Fe and Co L_3 edges (Figure S3, SI). They bear the signature of Fe^{II}_{LS} and Co^{III}_{LS} ions with small contributions from Fe^{III}_{LS} and Co^{II}_{HS} ions. At 300 K, the two spectra recorded at the beginning and at the very end of the temperature cycle exhibit the clear signature of Fe^{III}_{LS} and Co^{II}_{HS} metal ions (Figure S4, SI). This confirms unambiguously the complete reversibility of the electron transfer process for both the temperature-induced and the light-induced conversions. In other words, there is no sign of any sample degradation under X-ray or 660 nm irradiations.

For completeness, the Fe and Co K edges XAS spectra were recorded for **1** at 300 and at 4 K before and after light irradiation. Since the escape depth for hard X-ray photons at the Fe and Co K edges is larger than 10 μm, the obtained information relates to the bulk of the sample. On the contrary,

DOI: 10.1021/jacs.8b10484
J. Am. Chem. Soc. 2019, 141, 3470–3479

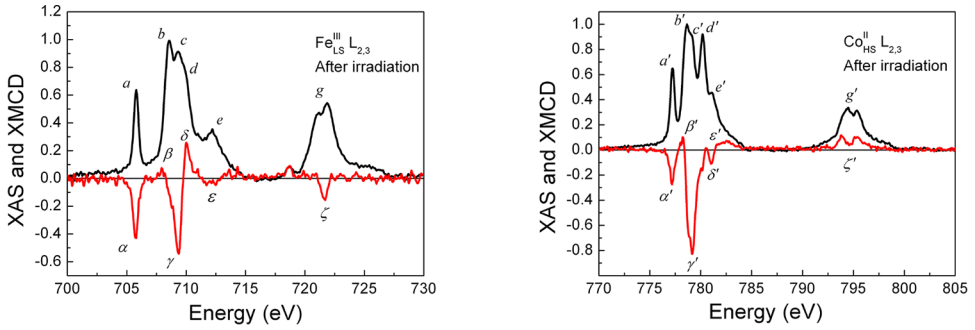

Figure 5. Experimental XAS (black line) and XMCD (red line) signals at the Fe (left) and Co (right) $L_{2,3}$ edges at T = 2 K and **B** = 6.5 T after 660 nm irradiation, in compound **1**.

when the Fe and Co $L_{2,3}$ edges are measured in TEY, the escape depth of the electrons is not larger than 5 nm, so that the probed sample is essentially the very surface of the sample. The whole set of results for K edges is presented in the Supporting Information (Figures S5, S6, S7, and S8) and the conclusions are very similar to the ones obtained at the Fe and Co $L_{2,3}$ edges.

From the comparison with experimental spectra[54] or theoretical ones,[41,75] we have been able to characterize the different electronic states (high temperature, low temperature, and after light irradiation) of **1** for both Co and Fe ions. We have confirmed with soft and hard X-rays that the thermally induced and the light-induced metal-to-metal electron transfer is accompanied by an electronic reorganization at the Co site from a LS configuration for Co(III) to a HS configuration for Co(II).

Magnetic Properties of the Light-Induced Excited State. XMCD spectra have been recorded at the Fe and Co $L_{2,3}$ edges at 2 K after photoexcitation, in an external magnetic induction of 6.5 T (Figure 5). For normalization, the background was subtracted from the XAS spectra using two arctangent functions that model the $2p_{3/2}\rightarrow$ continuum and $2p_{1/2}\rightarrow$ continuum transitions.[76] Then the maximum of the L_3 edge is set to 1 and the XMCD signal is normalized in proportion. The large intensity of the Fe L_2 edge on the XAS signal is a clear indication that the Fe ion is in a low-spin state,[77,78] while the relatively small Co L_2 edge is a sign that Co ions are in their high-spin state. XMCD signals at the Fe L_3 and the Co L_3 edges are both negative, which evidence that Fe and Co total magnetic moments point in the same direction at T = 2 K and **B** = 6.5 T. In such conditions, there is no indication of an antiferromagnetic coupling between Fe and Co magnetic moments.

The XMCD signal at the Fe $L_{2,3}$ edges has three main negative features, α, γ, ζ, and two moderately positive ones, β and δ. Its intensity is not small, since the γ feature amounts to 57% of the maximum of the L_3 edge. Thus, from the shape and intensity of XMCD, one expects a rather large orbital magnetic moment that is likely to overcome the spin magnetic moment. The spin sum rule is known to be nonvalid for the $L_{2,3}$ edges of Fe^{III}_{LS}, so that the Fe spin magnetic moment can only be determined by LFM calculations or by comparison with reference XMCD data.[74] From the experimental XMCD signal recorded for **2** and from LFM calculations where the back-bonding character of the cyanido bonding is fully taken into account, it is determined by cross-multiplication that the orbit and spin magnetic moments of Fe^{III}_{LS} in **1** are equal to ≈0.65 μ_B and ≈0.53 μ_B, respectively (left panel of Figure S9, SI). The XMCD signal at the Co L_3 edge is characterized by a large negative contribution, γ', accompanied by two smaller negative ones, α' and δ', while the XMCD signal at the L_2 edge gives a small positive contribution. The intensity of the γ' peak is rather large and amounts to 83% of the maximum of the Co L_3 edge spectrum. One thus expects a rather large magnetic moment carried by the Co ions with a significant contribution from the orbital magnetic moment. By comparison with LFM calculations, one finds that the orbital magnetic moment is 0.46 μ_B and the spin magnetic one is 1.38 μ_B per Co ion (left panel of Figure S10, SI).

For compound **1**, the magnetization curves detected by XMCD independently for Fe and Co ions are shown in Figure 6. They have been recorded by setting the monochromator at

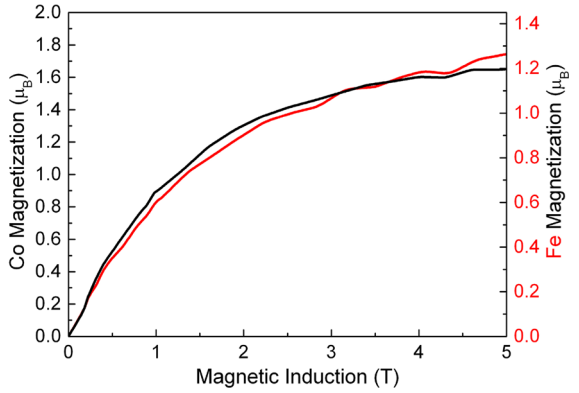

Figure 6. Field dependence of the maximum of the XMCD signal at the L_3 edge for Fe (red line) and Co (black line). The XMCD intensity is converted into Bohr magnetons following the magnetic moment determination from Figure 5 (see the text for more information).

the maximum of the L_3 edge XMCD signals for Fe (at 709.33 eV) and Co (at 779.18 eV), ramping up and down the magnetic field between +5 and −5 T. The various magnetization branches have been properly averaged to yield the 0−5 T magnetization curve and have been normalized in Bohr magnetons, in agreement with the Fe and Co magnetic moments determined by XMCD. The magnetic saturation is not completely achieved for both Fe and Co ions, and no detectable opening of the magnetization curves is observed. In addition, the shapes of the magnetization curves are very similar for both Fe and Co, so that there is no sign of any antiferromagnetic coupling between the two ions at T = 2 K. It is not possible from the present set of magnetization curves to determine if the Fe and Co ions are ferromagnetically coupled

DOI: 10.1021/jacs.8b10484
J. Am. Chem. Soc. 2019, 141, 3470−3479

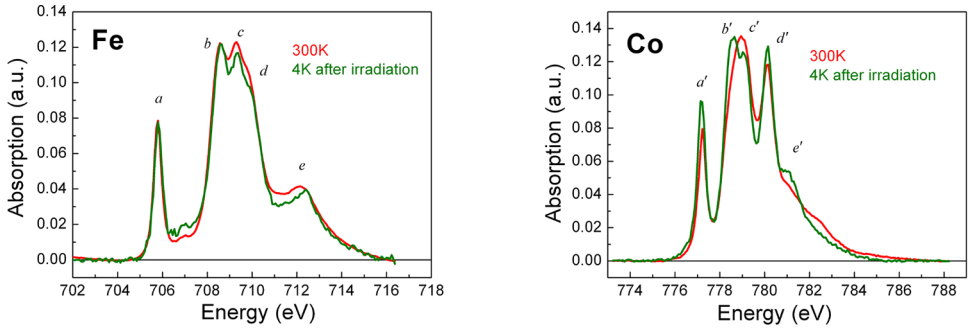

Figure 7. XAS spectra measured at the Fe (left) and Co (right) L_3 edges at 300 K before irradiation (red line) and at 4 K after irradiation (green line).

or if they simply experience a similar magnetization under the action of the external magnetic induction.

DISCUSSION

The present experimental results clearly evidence that the temperature-induced magnetic conversion between 300 and 100 K corresponds to an electron transfer that transforms the Fe^{III}_{LS}–Co^{II}_{HS} paramagnetic pair into its Fe^{II}_{LS}–Co^{III}_{LS} diamagnetic analogue. At lower temperature, around 4 K, the Fe^{II}_{LS}–Co^{III}_{LS} diamagnetic pair can be transformed into the Fe^{III}_{LS}–Co^{II}_{HS} paramagnetic pair under light irradiation. This result is fully in line with what is claimed by Koumousi et al.[37] from conventional magnetic susceptibility measurements on the same system. Nevertheless, we want to stress that the present work reports the first direct evidence of the respective electronic state of Fe and Co ions at the atomic scale and this for all the different phases involved in the switching mechanism. This conclusion is absolutely unambiguous, since the spectral features associated with the XAS spectra at the $L_{2,3}$ edges of Fe^{II}_{LS}, Fe^{III}_{LS}, Co^{II}_{HS}, and Co^{III}_{LS} are well-documented in the literature from experimental reference spectra as well as from theoretical spectra calculated in the LFM model.[42,55,71−73,79,80] In addition, the qualitative analysis of the features at the K edges support this conclusion, although quantitative results are more difficult to extract.

At T = 100 K, it was found that the temperature-induced magnetic conversion was not complete. This is regularly observed when temperature- or light-induced conversions are observed by XAS at $L_{2,3}$ edges measured in TEY, where the probing depth is less than 5 nm. Indeed, depending on the samples, Poneti et al. observed between 50 and 60% of residual high-temperature phase at 100 K,[42,53,81] and Warner et al. observed between 10 and 55% of residual depending on the sample thickness.[49] The temperature-induced magnetic switching is possible when the environment of the Co ions allows enough flexibility so that the site can accommodate a Co^{II}_{HS} to Co^{III}_{LS} conversion.[54,73,79] At the very surface of the measured sample, it is likely that the Co coordination sphere undergoes a partial reorganization that might prevent the temperature-induced electron transfer, explaining the observed residual contribution.

At 300 K and at 4 K after irradiation, **1** is composed of Fe^{III}_{LS}–Co^{II}_{HS} paramagnetic pairs. From the comparison of both XAS spectra at the Fe $L_{2,3}$ edges, one can conclude that the electronic and local structures of Fe at 300 K are very similar to those at 4 K after irradiation (Figure 7, left panel). On the contrary, a similar comparison for the Co $L_{2,3}$ edges clearly indicates that the two Co^{II}_{HS} spectra at 300 K and at 4 K are quite different: for the latter, feature a' is sharper, the intensities of features b' and c' are reversed, and feature e' is larger (Figure 7, right panel). These differences cannot originate from an incomplete photomagnetic conversion, since feature a' is more intense for the 4 K spectrum than for the 300 K one. They might arise either from a temperature dependence of the Co $L_{2,3}$ edges spectra or from local rearrangements around the Co ions similar to the ones observed for 3-D PBA molecule-based magnets.[55,72,73,79] Therefore, XAS spectra were calculated in the LFM model for a Co^{II}_{HS} ion in the same environment at 4 and 300 K, i.e., for the same set of crystal-field and spin-orbit parameters (Table S1, SI). From Figure S11 (SI), it is clear that the calculations mimic fairly well the differences observed between the experimental Co XAS spectra for the two temperatures. On the basis of the LFM calculations, it can therefore be concluded that the parameters governing the electronic structure of Co^{II}_{HS} ions such as spin-orbit coupling, crystal field, and site distortion are likely identical in the 300 K paramagnetic phase and in the 4 K photoinduced phase. The difference in the electronic structure between 300 and 4 K stems from the different thermal population of the first excited states. This is in agreement with the K edge XAS and XRD results reported by Sekine et al. in cyanido-bridged FeCo square molecules, where they confirmed that the electronic structure of the low-temperature light-induced state is similar to that of the high-temperature state.[43,59]

In Figure 6, the XMCD-detected magnetization curves for Fe and Co ions are superimposed. Within the uncertainty of the experimental measurement, there is no hint of antiferromagnetic coupling between Fe^{III}_{LS} and Co^{II}_{HS} magnetic sites, in contrast to what has been suggested for similar systems.[37,57,82] Since measurements have been performed at 2 K, our results indicate that the exchange coupling constant (J) between Fe and Co ions is such that $|J/k_B| \ll 1$ K (for $H = -2J\vec{S}_{Fe}\ \vec{S}_{Co}$).

In order to gain more information on the fine electronic structures of Fe and Co ions in the low-temperature, photoinduced state, the XAS and XMCD signals from the two precursors (compounds **2** and **3**; see the Experimental Section) of **1** were recorded at 2 K and in an external magnetic induction of 6.5 T. The Fe $L_{2,3}$ edges for compounds **1** and **2** are very similar (Figure S9, SI). One observes the same series of spectral features, with mainly peak a that is characteristic of Fe^{III}_{LS} and shoulder e that is a signature of Fe surrounded by three cyanido ligands. The intensity of features b, c, and d are rather different, as can be expected from the presence of the (Fe−CN−Co) bridge in **1**. The XMCD features are also very

DOI: 10.1021/jacs.8b10484
J. Am. Chem. Soc. 2019, 141, 3470−3479

similar and almost homothetic for both samples. If one focuses on features *a* in the XAS spectra and α in the XMCD signals, the ratio α/a is 66% for **1**, while it is 70% for its precursor **2**.[74] For compounds **1** and **3**, the situation is somewhat different at the Co L_3 edge. Indeed the local organization of the Co ions is very different in these compounds, so that both Co XAS spectra are quite different (Figure S10, SI). In contrast, the two Co XMCD signals present similarities at the L_3 edge and rather large differences at the L_2 edge. The general shape is in agreement with what is expected for a hexacoordinated Co^{II}_{HS} ion. One then concludes that, at 6.5 T, the magnetizations of Fe and Co ions in **1** are quite similar to the magnetizations for isolated paramagnetic ions, as is the case in **2** and **3**. This again confirms that the thermal fluctuations at 2 K are larger than any significant antiferromagnetic coupling between Fe and Co ions in **1**.

CONCLUSIONS

The electronic and magnetic structures of Fe and Co ions in a dinuclear photomagnetic PBA have been measured for the first time in an element-selective way. Using a combination of XAS and XMCD spectroscopies supported by LFM calculations, our results prove unambiguously that (i) the 300 K phase and the light-induced excited state at 4 K are composed of Fe^{III}_{LS}–Co^{II}_{HS} paramagnetic pairs and (ii) the 100 K phase is involving Fe^{II}_{LS}–Co^{III}_{LS} diamagnetic pairs. From the LFM calculations, one can suggest that both paramagnetic phases at 300 K and at 4 K after light irradiation are identical, with no apparent major reorganization of the local structure around either Fe or Co. In the paramagnetic pairs at 2 K and under an external magnetic induction of 6.5 T, both Fe and Co ions exhibit rather large orbital magnetic moments: 0.65 μ_B for Fe and 0.46 μ_B for Co. For Fe ions, the orbital magnetic moment is larger than the spin magnetic moment, as already observed for the $[TpFe(CN)_3]^-$ precursor, i.e., **2**.[74] The total magnetic moment of Co is larger than the Fe one, and we do not observe any evidence of antiferromagnetic coupling between Fe and Co magnetic centers. The light-induced excited state is relaxed at 50 K, so that at temperatures below 50 K, **1** presents a bistability that could be addressed by an appropriate application of light and temperature. XMCD measurements at very low temperature (around 200 mK)[61] might help further characterizing the sign and magnitude of the magnetic coupling between Fe and Co metal ions.

Understanding the electron transfer mechanism in the dinuclear PBA **1** was a necessary first step before exploring whether this molecule or similar ones would preserve the electron transfer mechanism when isolated on surfaces. Such future studies could pave the way toward ultimate miniaturization.

ASSOCIATED CONTENT

Supporting Information

The Supporting Information is available free of charge on the ACS Publications website at DOI: 10.1021/jacs.8b10484.

XAS spectra at the $L_{2,3}$ edges showing the reversibility, XAS spectra measured at the Fe and Co K edges, XAS and XMCD spectra measured in the Fe and Co precursors, and Co L_3 edge spectra calculated in the ligand field multiplet model (PDF)

AUTHOR INFORMATION

Corresponding Authors

*Marie-Anne.Arrio@sorbonne-universite.fr
*Corine.Mathoniere@icmcb.cnrs.fr
*Philippe.Sainctavit@sorbonne-universite.fr

ORCID

Marie-Anne Arrio: 0000-0002-2945-6824
Amélie Juhin: 0000-0003-0752-3034
Dmitri Mitcov: 0000-0003-2435-1174
Dongfeng Li: 0000-0001-6537-3279
Rodolphe Clérac: 0000-0001-5429-7418
Philippe Sainctavit: 0000-0001-9349-2558

Notes

The authors declare no competing financial interest.

ACKNOWLEDGMENTS

This work was supported by the Centre National de la Recherche Scientifique (CNRS, France), the Ministère de l' Enseignement Supérieur et de la Recherche (MESR, France), NNSF of the People's Republic of China (No. 21471063, 21172084), the Nouvelle Aquitaine region, the Institut Universitaire de France (IUF) and partially funded by ANR (ANR-10-BLAN-0712; ANR-09-BLAN-0175; ANR-12-PDOC-0038), the GDR MCM2 (Magnétisme et commutation moléculaires), and the MOLSPIN COST action CA15128. The staff from SOLEIL, SLS, and ESRF is acknowledged for operating the synchrotron sources and beamlines. We are glad to acknowledge Dr. Armin Kleibert for his technical support on the SIM beamline. We also thank Bernard Muller (IPCMS, Strasbourg) for instrumental developments on the French TBT-mK dilution cryomagnet.

REFERENCES

(1) Sanvito, S. Molecular Spintronics. *Chem. Soc. Rev.* **2011**, *40*, 3336–3355.
(2) Gatteschi, D.; Sessoli, R. Molecular Nanomagnets: The First 10 Years. *J. Magn. Magn. Mater.* **2004**, *272–276*, 1030–1036.
(3) Joachim, C.; Gimzewski, J. K.; Aviram, A. Electronics using Hybrid-Molecular and Mono-Molecular Devices. *Nature* **2000**, *408*, 541–548.
(4) Camarero, J.; Coronado, E. Molecular vs. Inorganic Spintronics: The Role of Molecular Materials and Single Molecules. *J. Mater. Chem.* **2009**, *19*, 1678–1684.
(5) Leuenberger, M. N.; Loss, D. Quantum Computing in Molecular Magnets. *Nature* **2001**, *410*, 789–793.
(6) Miyamachi, T.; Gruber, M.; Davesne, V.; Bowen, M.; Boukari, S.; Joly, L.; Scheurer, F.; Rogez, G.; Yamada, T. K.; Ohresser, P.; Beaurepaire, E.; Wulfhekel, W. Robust Spin Crossover and Memristance Across a Single Molecule. *Nat. Commun.* **2012**, *3*, 938.
(7) Kompa, K. L.; Levine, R. D. A Molecular Logic Gate. *Proc. Natl. Acad. Sci. U. S. A.* **2001**, *98*, 410–414.
(8) Andréasson, J.; Pischel, U.; Straight, S. D.; Moore, T. A.; Moore, A. L.; Gust, D. All-Photonic Multifunctional Molecular Logic Device. *J. Am. Chem. Soc.* **2011**, *133*, 11641–11648.
(9) Sato, O. Optically Switchable Molecular Solids: Photoinduced Spin-Crossover, Photochromism, and Photoinduced Magnetization. *Acc. Chem. Res.* **2003**, *36*, 692–700.
(10) Bonhommeau, S.; Molnár, G.; Galet, A.; Zwick, A.; Real, J.-A.; McGarvey, J. J.; Bousseksou, A. One Shot Laser Pulse Induced Reversible Spin Transition in the Spin-Crossover Complex $[Fe(C_4H_4N_2)Pt(CN)_4]$ at Room Temperature. *Angew. Chem., Int. Ed.* **2005**, *44*, 4069–4073.
(11) Sato, O. Photoinduced Magnetization in Molecular Compounds. *J. Photochem. Photobiol., C* **2004**, *5*, 203–223.

DOI: 10.1021/jacs.8b10484
J. Am. Chem. Soc. 2019, 141, 3470–3479

(12) Aguilá, D.; Prado, Y.; Koumousi, E. S.; Mathonière, C.; Clérac, R. Switchable Fe/Co Prussian Blue Networks and Molecular Analogues. *Chem. Soc. Rev.* **2016**, *45*, 203−224.
(13) Sato, O.; Iyoda, T.; Fujishima, A.; Hashimoto, K. Photoinduced Magnetization of a Cobalt-Iron Cyanide. *Science* **1996**, *272*, 704−705.
(14) Sato, O.; Einaga, Y.; Fujishima, A.; Hashimoto, K. Photoinduced Long-Range Magnetic Ordering of a Cobalt Iron Cyanide. *Inorg. Chem.* **1999**, *38*, 4405−4412.
(15) Sato, O.; Tao, J.; Zhang, Y.-Z. Control of Magnetic Properties through External Stimuli. *Angew. Chem., Int. Ed.* **2007**, *46*, 2152−2187.
(16) Sato, O. Switchable Molecular Magnets. *Proc. Jpn. Acad., Ser. B* **2012**, *88*, 213−225.
(17) Verdaguer, M. Molecular Electronics Emerges from Molecular Magnetism. *Science* **1996**, *272*, 698.
(18) Ksenofontov, V.; Levchenko, G.; Reiman, S.; Gütlich, P.; Bleuzen, A.; Escax, V.; Verdaguer, M. Pressure-Induced Electron Transfer in Ferrimagnetic Prussian Blue Analogs. *Phys. Rev. B: Condens. Matter Mater. Phys.* **2003**, *68*, No. 024415.
(19) Zhan, S.-z.; Chen, X.-y.; Meng, Q.-j.; Xei, W. Synthesis, Characterization and Electrochemical Properties of Cyanide-Bridged Cobalt(III)/Iron(II) Complexes. *Synth. React. Inorg. Met.-Org. Chem.* **1996**, *26*, 277−284.
(20) Bernhardt, P. V.; Martinez, M. The First Structurally Characterized Discrete Dinuclear μ-Cyano Hexacyanoferrate Complex. *Inorg. Chem.* **1999**, *38*, 424−425.
(21) Bernhardt, P. V.; Macpherson, B. P.; Martinez, M. Discrete Dinuclear Cyano-Bridged Complexes. *Inorg. Chem.* **2000**, *39*, 5203−5208.
(22) Berlinguette, C. P.; Dragulescu-Andrasi, A.; Sieber, A.; Galán-Mascarós, J. R.; Güdel, H.-U.; Achim, C.; Dunbar, K. R. A Charge-Transfer-Induced Spin Transition in the Discrete Cyanide-Bridged Complex $\{[Co(tmphen)_2]_3Fe(CN)_6]_2\}$. *J. Am. Chem. Soc.* **2004**, *126*, 6222−6223.
(23) Funck, K. E.; Prosvirin, A. V.; Mathonière, C.; Clérac, R.; Dunbar, K. R. Light-Induced Excited Spin State Trapping and Charge Transfer in Trigonal Bipyramidal Cyanide- Bridged Complexes. *Inorg. Chem.* **2011**, *50*, 2782−2789.
(24) Li, D.; Parkin, S.; Wang, G.; Yee, G. T.; Holmes, S. M. Synthesis and Spectroscopic and Magnetic Characterization of Tris(3,5-dimethylpyrazol-1-yl)borate Iron Tricyanide Building Blocks, a Cluster, and a One-Dimensional Chain of Squares. *Inorg. Chem.* **2006**, *45*, 1951−1959.
(25) Liu, T.; Zhang, Y.-J.; Kanegawa, S.; Sato, O. Photoinduced Metal-to-Metal Charge Transfer toward Single-Chain Magnet. *J. Am. Chem. Soc.* **2010**, *132*, 8250−8251.
(26) Hoshino, N.; Iijima, F.; Newton, G. N.; Yoshida, N.; Shiga, T.; Nojiri, H.; Nakao, A.; Kumai, R.; Murakami, Y.; Oshio, H. Three-Way Switching in a Cyanide-Bridged [CoFe] chain. *Nat. Chem.* **2012**, *4*, 921−926.
(27) Baker, M. L.; Kitagawa, Y.; Nakamura, T.; Tazoe, K.; Narumi, Y.; Kotani, Y.; Iijima, F.; Newton, G. N.; Okumura, M.; Oshio, H.; Nojiri, H. X-ray Magnetic Circular Dichroism Investigation of the Electron Transfer Phenomena Responsible for Magnetic Switching in a Cyanide-Bridged [CoFe] Chain. *Inorg. Chem.* **2013**, *52*, 13956−13962.
(28) Jiang, W.; Jiao, C.; Meng, Y.; Zhao, L.; Liu, Q.; Liu, T. Switching single chain magnet behavior via photoinduced bidirectional metal-to-metal charge transfer. *Chem. Sci.* **2018**, *9*, 617−622.
(29) Li, D.; Clérac, R.; Roubeau, O.; Harté, E.; Mathonière, C.; Le Bris, R.; Holmes, S. M. Magnetic and Optical Bistability Driven by Thermally and Photoinduced Intramolecular Electron Transfer in a Molecular Cobalt-Iron Prussian Blue Analogue. *J. Am. Chem. Soc.* **2008**, *130*, 252−258.
(30) Zhang, Y.; Li, D.; Clérac, R.; Kalisz, M.; Mathonière, C.; Holmes, S. M. Reversible Thermally Photoinduced Electron Transfer in a Cyano-Bridged $\{Fe_2Co_2\}$ Square Complex. *Angew. Chem., Int. Ed.* **2010**, *49*, 3752−3756.
(31) Mercurol, J.; Li, Y.; Pardo, E.; Risset, O.; Seuleiman, M.; Rousselière, H.; Lescouëzec, R.; Julve, M. $[Fe^{II}_{LS}Co^{III}_{LS}]_2$ - $[Fe^{III}_{LS}Co^{II}_{HS}]_2$ photoinduced conversion in a cyanide-bridged heterobimetallic molecular square. *Chem. Commun.* **2010**, *46*, 8995−8997.
(32) Zhang, Y.-Z.; Ferko, P.; Siretanu, D.; Ababei, R.; Rath, N. P.; Shaw, M. J.; Clérac, R.; Mathonière, C.; Holmes, S. M. Thermochromic and Photoresponsive Cyanometalate Fe/Co Squares: Toward Control of the Electron Transfer Temperature. *J. Am. Chem. Soc.* **2014**, *136*, 16854−16864.
(33) Mondal, A.; Li, Y.; Seuleiman, M.; Julve, M.; Toupet, L.; Buron-Le Cointe, M.; Lescouëzec, R. On/Off Photoswitching in a Cyanide-Bridged $\{Fe_2Co_2\}$ Magnetic Molecular Square. *J. Am. Chem. Soc.* **2013**, *135*, 1653−1656.
(34) Nihei, M.; Yanai, Y.; Hsu, I. J.; Sekine, Y.; Oshio, H. A Hydrogen-Bonded Cyanide-Bridged $[Co_2Fe_2]$ Square Complex Exhibiting a Three-Step Spin Transition. *Angew. Chem., Int. Ed.* **2017**, *56*, 591−594.
(35) Sekine, Y.; Nihei, M.; Oshio, H. Dimensionally Controlled Assembly of an External Stimuli-Responsive $[Co_2Fe_2]$ Complex into Supramolecular Hydrogen-Bonded Networks. *Chem. - Eur. J.* **2017**, *23*, 5193−5197.
(36) Jeon, I.-R.; Calancea, S.; Panja, A.; Piñero Cruz, D. M.; Koumousi, E. S.; Dechambenoit, P.; Coulon, C.; Wattiaux, A.; Rosa, P.; Mathonière, C.; Clérac, R. Spin Crossover or Intra-Molecular Electron Transfer in a Cyanido-Bridged Fe/Co Dinuclear Dumbbell: A Matter of State. *Chem. Sci.* **2013**, *4*, 2463−2470.
(37) Koumousi, E. S.; Jeon, I.-R.; Gao, Q.; Dechambenoit, P.; Woodruff, D. N.; Merzeau, P.; Buisson, L.; Jia, X.; Li, D.; Volatron, F.; Mathonière, C.; Clérac, R. Metal-to-Metal Electron Transfer in Co/Fe Prussian Blue Molecular Analogues: The Ultimate Miniaturization. *J. Am. Chem. Soc.* **2014**, *136*, 15461−15464.
(38) Nihei, M.; Sekine, Y.; Suganami, N.; Oshio, H. Thermally Two-stepped Spin Transitions Induced by Intramolecular Electron Transfers in a Cyanide-bridged Molecular Square. *Chem. Lett.* **2010**, *39*, 978−979.
(39) Mathonière, C. Metal-to-Metal Electron Transfer: A Powerful Tool for the Design of Switchable Coordination Compounds. *Eur. J. Inorg. Chem.* **2018**, *2018* (3−4), 248−258.
(40) Meng, Y.-S.; Sato, O.; Liu, T. Manipulating Metal-to-Metal Charge Transfer for Materials with Switchable Functionality. *Angew. Chem., Int. Ed.* **2018**, *57*, 12216−12226.
(41) Poneti, G.; Mannini, M.; Sorace, L.; Sainctavit, P.; Arrio, M.-A.; Rogalev, A.; Wilhelm, F.; Dei, A. X-ray Absorption Spectroscopy as a Probe of Photo- and Thermally Induced Valence Tautomeric Transition in a 1:1 Cobalt-Dioxolene Complex. *ChemPhysChem* **2009**, *10*, 2090−2095.
(42) Poneti, G.; Mannini, M.; Sorace, L.; Sainctavit, P.; Arrio, M.-A.; Otero, E.; Criginski Cezar, J.; Dei, A. Soft-X-ray-Induced Redox Isomerism in a Cobalt Dioxolene Complex. *Angew. Chem., Int. Ed.* **2010**, *49*, 1954−1957.
(43) Sekine, Y.; Nihei, M.; Kumai, R.; Nakao, H.; Murakami, Y.; Oshio, H. Investigation of the Light-Induced Electron-Transfer-Coupled Spin Transition in a Cyanide-Bridged $[Co_2Fe_2]$ Complex by X-ray Diffraction and Absorption Measurements. *Inorg. Chem. Front.* **2014**, *1*, 540−543.
(44) Jafri, S. F.; Arrio, M.-A.; Bordage, A.; Moulin, R.; Juhin, A.; Cartier dit Moulin, C.; Otero, E.; Ohresser, P.; Bleuzen, A.; Sainctavit, P. Weak Ferromagnetic Interaction at the Surface of the Ferrimagnetic $Rb_2Co_4[Fe(CN)_6]_{3.3}$:11H_2O Photoexcited State. *Inorg. Chem.* **2018**, *57*, 7610−7619.
(45) Bordage, A.; Moulin, R.; Fonda, E.; Fornasieri, G.; Rivière, E.; Bleuzen, A. Evidence of the Core-Shell Structure of (Photo)magnetic CoFe Prussian Blue Analogue Nanoparticles and Peculiar Behavior of the Surface Species. *J. Am. Chem. Soc.* **2018**, *140*, 10332−10343.
(46) de Groot, F. M. F.; Fuggle, J. C.; Thole, B. T.; Sawatzky, G. A. 2*p* X-ray Absorption of 3*d* Transition-Metal Compounds: An Atomic Multiplet Description Including the Crystal Field. *Phys. Rev. B: Condens. Matter Mater. Phys.* **1990**, *42*, 5459−5468.

DOI: 10.1021/jacs.8b10484
J. Am. Chem. Soc. 2019, 141, 3470−3479

(47) Thole, B. T.; Carra, P.; Sette, F.; van der Laan, G. X-ray Circular Dichroism as a Probe of Orbital Magnetization. *Phys. Rev. Lett.* **1992**, *68*, 1943−1946.
(48) Carra, P.; Thole, B. T.; Altarelli, M.; Wang, X. X-ray Circular Dichroism and Local Magnetic Fields. *Phys. Rev. Lett.* **1993**, *70*, 694−697.
(49) Warner, B.; Oberg, J. C.; Gill, T. G.; El Hallak, F.; Hirjibehedin, C. F.; Serri, M.; Heutz, S.; Arrio, M.-A.; Sainctavit, P.; Mannini, M.; Poneti, G.; Sessoli, R.; Rosa, P. Temperature- and Light-Induced Spin Crossover Observed by X-ray Spectroscopy on Isolated Fe(II) Complexes on Gold. *J. Phys. Chem. Lett.* **2013**, *4*, 1546−1552.
(50) Davesne, V.; Gruber, M.; Miyamachi, T.; Da Costa, V.; Boukari, S.; Scheurer, F.; Joly, L.; Ohresser, P.; Otero, E.; Choueikani, F.; Gaspar, A. B.; Real, J. A.; Wulfhekel, W.; Bowen, M.; Beaurepaire, E. First Glimpse of the Soft X-ray Induced Excited Spin-State Trapping Effect Dynamics on Spin Cross-Over Molecules. *J. Chem. Phys.* **2013**, *139*, No. 074708.
(51) Briois, V.; Cartier dit Moulin, C.; Sainctavit, P.; Brouder, C.; Flank, A.-M. Full Multiple Scattering and Crystal Field Multiplet Calculations Performed on the Spin Transition $Fe^{II}(phen)_2(NCS)_2$ Complex at the Iron K and $L_{2,3}$ X-ray Absorption Edges. *J. Am. Chem. Soc.* **1995**, *117*, 1019−1026.
(52) Dapporto, P.; Dei, A.; Poneti, G.; Sorace, L. Complete Direct and Reverse Optically Induced Valence Tautomeric Interconversion in a Cobalt-Dioxolene Complex. *Chem. - Eur. J.* **2008**, *14*, 10915−10918.
(53) Poneti, G.; Mannini, M.; Cortigiani, B.; Poggini, L.; Sorace, L.; Otero, E.; Sainctavit, P.; Sessoli, R.; Dei, A. Magnetic and Spectroscopic Investigation of Thermally and Optically Driven Valence Tautomerism in Thioether-Bridged Dinuclear Cobalt−Dioxolene Complexes. *Inorg. Chem.* **2013**, *52*, 11798−11805.
(54) Bleuzen, A.; Lomenech, C.; Escax, V.; Villain, F.; Varret, F.; Cartier dit Moulin, C.; Verdaguer, M. Photoinduced Ferrimagnetic Systems in Prussian Blue Analogues $C^I_x\ Co_4[Fe(CN)_6]_y$ (C^I = Alkali Cation). 1. Conditions to Observe the Phenomenon. *J. Am. Chem. Soc.* **2000**, *122*, 6648−6652.
(55) Cartier dit Moulin, C.; Villain, F.; Bleuzen, A.; Arrio, M.-A.; Sainctavit, P.; Lomenech, C.; Escax, V.; Baudelet, F.; Dartyge, E.; Gallet, J.-J.; Verdaguer, M. Photoinduced Ferrimagnetic Systems in Prussian Blue Analogues $C^I_xCo_4[Fe(CN)_6]_y$ (C^I = Alkali Cation). 2. X-ray Absorption Spectroscopy of the Metastable State. *J. Am. Chem. Soc.* **2000**, *122*, 6653−6658.
(56) Escax, V.; Bleuzen, A.; Cartier dit Moulin, C.; Villain, F.; Goujon, A.; Varret, F.; Verdaguer, M. Photoinduced Ferrimagnetic Systems in Prussian Blue Analogues $C^I_x\ Co_4[Fe(CN)_6]_y$ (C^I = Alkali Cation). 3. Control of the Photo- and Thermally Induced Electron Transfer by the $[Fe(CN)_6]$ Vacancies in Cesium Derivatives. *J. Am. Chem. Soc.* **2001**, *123*, 12536−12543.
(57) Champion, G.; Escax, V.; Cartier dit Moulin, C.; Bleuzen, A.; Villain, F.; Baudelet, F.; Dartyge, E.; Verdaguer, M. Photoinduced Ferrimagnetic Systems in Prussian Blue Analogues $C^I_x\ Co_4[Fe(CN)_6]_y$ (C^I = Alkali Cation). 4. Characterization of the Ferrimagnetism of the Photoinduced Metastable State by K Edges X-ray Magnetic Circular Dichroism. *J. Am. Chem. Soc.* **2001**, *123*, 12544−12546.
(58) Yokoyama, T.; Kiguchi, M.; Ohta, T.; Sato, O.; Einaga, Y.; Hashimoto, K. Local Structure of a Trapped Photoexcited State of a Fe-Co cyanide studied by X-ray-Absorption Fine-Structure Spectroscopy. *Phys. Rev. B: Condens. Matter Mater. Phys.* **1999**, *60*, 9340−9346.
(59) Sekine, Y.; Nihei, M.; Kumai, R.; Nakao, H.; Murakami, Y.; Oshio, H. X-ray-induced Phase Transitions by Selective Excitation of Heterometal Ions in a Cyanide-Bridged Fe−Co Molecular Square. *Chem. Commun.* **2014**, *50*, 4050−4052.
(60) Ohresser, P.; Otero, E.; Choueikani, F.; Chen, K.; Stanescu, S.; Deschamps, F.; Moreno, T.; Polack, F.; Lagarde, B.; Daguerre, J.-P.; Marteau, F.; Scheurer, F.; Joly, L.; Kappler, J.-P.; Muller, B.; Bunau, O.; Sainctavit, P. DEIMOS: A Beamline Dedicated to Dichroism Measurements in the 350−2500 eV Energy Range. *Rev. Sci. Instrum.* **2014**, *85*, No. 013106.
(61) Letard, I.; Sainctavit, P.; dit Moulin, C. C.; Kappler, J.-P.; Ghigna, P.; Gatteschi, D.; Doddi, B. Remnant Magnetization of Fe_8 High-Spin Molecules: X-ray Magnetic Circular Dichroism at 300 mK. *J. Appl. Phys.* **2007**, *101*, 113920.
(62) Mannini, M.; Pineider, F.; Sainctavit, P.; Joly, L.; Fraile-Rodríguez, A.; Arrio, M.- A.; Cartier dit Moulin, C.; Wernsdorfer, W.; Cornia, A.; Gatteschi, D.; Sessoli, R. X-Ray Magnetic Circular Dichroism Picks out Single-Molecule Magnets Suitable for Nanodevices. *Adv. Mater.* **2009**, *21*, 167−171.
(63) Goulon, J.; Rogalev, A.; Wilhelm, F.; Jaouen, N.; Goulon-Ginet, C.; Brouder, C. Optical Activity Probed with X-rays. *J. Phys.: Condens. Matter* **2003**, *15*, S633.
(64) Goulon, J.; Rogalev, A.; Gauthier, C.; Goulon-Ginet, C.; Paste, S.; Signorato, R.; Neumann, C.; Varga, L.; Malgrange, C. Instrumentation Developments for X-ray Linear and Circular Dichroism at the ESRF Beamline ID12A. *J. Synchrotron Radiat.* **1998**, *5*, 232−238.
(65) Brouder, C.; Kappler, J.-P. Prolegomena to Magnetic Circular Dichroism in X-ray Absorption Spectroscopy. In *Magnetism and Synchrotron Radiation*; Springer, 1997; pp 19−32
(66) de Groot, F. M. F. Multiplet Effects in X-ray Spectroscopy. *Coord. Chem. Rev.* **2005**, *249*, 31−63.
(67) de Groot, F. M. F.; Kotani, A. *Core Level Spectroscopy of Solids*; CRC Press, 2008.
(68) Cowan, R. D. *The Theory of Atomic Structure and Spectra*; University of California Press: Berkeley, CA, 1981; Vol. 3.
(69) Butler, P. H. *Point Group Symmetry Applications: Methods and Tables*; Springer Science & Business Media: New York, 2012.
(70) Juhin, A.; Brouder, C.; Arrio, M.-A.; Cabaret, D.; Sainctavit, P.; Balan, E.; Bordage, A.; Seitsonen, A.; Calas, G.; Eeckhout, S.; Glatzel, P. X-ray Linear Dichroism in Cubic Compounds: The Case of Cr^{3+} in $MgAl_2O_4$. *Phys. Rev. B: Condens. Matter Mater. Phys.* **2008**, *78*, 195103.
(71) Hocking, R. K.; Wasinger, E. C.; de Groot, F. M. F.; Hodgson, K. O.; Hedman, B.; Solomon, E. I. Fe L-Edge XAS Studies of $K_4[Fe(CN)_6]$ and $K_3[Fe(CN)_6]$: A Direct Probe of Back-Bonding. *J. Am. Chem. Soc.* **2006**, *128*, 10442−10451.
(72) Escax, V.; Champion, G.; Arrio, M.-A.; Zacchigna, M.; Cartier dit Moulin, C.; Bleuzen, A. The Co Ligand Field: A Key Parameter in Photomagnetic CoFe Prussian Blue Derivatives. *Angew. Chem., Int. Ed.* **2005**, *44*, 4798−4801.
(73) Cartier dit Moulin, C.; Champion, G.; Cafun, J.-D.; Arrio, M.-A.; Bleuzen, A. Structural Rearrangements Induced by Photoexcitation in a RbCoFe Prussian Blue Derivative. *Angew. Chem., Int. Ed.* **2007**, *46*, 1287−1289.
(74) Jafri, S. F.; Koumousi, E. S.; Sainctavit, P.; Juhin, A.; Schuler, V.; Bunau, O.; Mitcov, D.; Dechambenoit, P.; Mathonière, C.; Clérac, R.; Otero, E.; Ohresser, P.; Cartier dit Moulin, C.; Arrio, M.-A. Large Orbital Magnetic Moment Measured in $[TpFe^{III}(CN)_6]^-$ the Precursor of Photomagnetic Molecular Prussian Blue Analogues. *Inorg. Chem.* **2016**, *55*, 6980−6987.
(75) Westre, T. E.; Kennepohl, P.; DeWitt, J. G.; Hedman, B.; Hodgson, K. O.; Solomon, E. I. A Multiplet Analysis of Fe K-edge 1s → 3d Pre-Edge Features of Iron Complexes. *J. Am. Chem. Soc.* **1997**, *119*, 6297−6314.
(76) Chen, C.-T.; Idzerda, Y. U.; Lin, H.-J.; Smith, N. V.; Meigs, G.; Chaban, E.; Ho, G. H.; Pellegrin, E.; Sette, F. Experimental Confirmation of the X-ray Magnetic Circular Dichroism Sum rules for Iron and Cobalt. *Phys. Rev. Lett.* **1995**, *75*, 152−155.
(77) Thole, B. T.; Van der Laan, G. Linear Relation between X-ray Absorption Branching Ratio and Valence-Band Spin-Orbit Expectation Value. *Phys. Rev. A: At., Mol., Opt. Phys.* **1988**, *38*, 1943−1947.
(78) Thole, B. T.; Van der Laan, G. Branching Ratio in X-ray Absorption Spectroscopy. *Phys. Rev. B: Condens. Matter Mater. Phys.* **1988**, *38*, 3158−3171.
(79) Cafun, J.-D.; Champion, G.; Arrio, M.-A.; Cartier dit Moulin, C.; Bleuzen, A. Photomagnetic CoFe Prussian Blue Analogues: Role of the Cyanide Ions as Active Electron Transfer Bridges Modulated by

DOI: 10.1021/jacs.8b10484
J. Am. Chem. Soc. 2019, 141, 3470−3479

Cyanide-Alkali Metal Ion Interactions. *J. Am. Chem. Soc.* **2010**, *132*, 11552−11559.
(80) Bonhommeau, S.; Pontius, N.; Cobo, S.; Salmon, L.; de Groot, F. M. F.; Molnár, G.; Bousseksou, A.; Dürr, H. A.; Eberhardt, W. Metal-to-Ligand and Ligand-to-Metal Charge Transfer in Thin Films of Prussian Blue Analogues Investigated by X-ray Absorption Spectroscopy. *Phys. Chem. Chem. Phys.* **2008**, *10*, 5882−5889.
(81) Poneti, G.; Poggini, L.; Mannini, M.; Cortigiani, B.; Sorace, L.; Otero, E.; Sainctavit, P.; Magnani, A.; Sessoli, R.; Dei, A. Thermal and Optical Control of Electronic States in a Single Layer of Switchable Paramagnetic Molecules. *Chem. Sci.* **2015**, *6*, 2268−2274.
(82) Goujon, A.; Roubeau, O.; Varret, F.; Dolbecq, A.; Bleuzen, A.; Verdaguer, M. Photo-Excitation from Dia- to Ferri-Magnetism in a Rb-Co-Hexacyanoferrate Prussian Blue Analogue. *Eur. Phys. J. B* **2000**, *14*, 115−124.

DOI: 10.1021/jacs.8b10484
J. Am. Chem. Soc. 2019, 141, 3470−3479